JOURNAL OF VIROLOGY, Feb. 2007, p. 1162–1173 Vol. 81, No. 3
0022-538X/07/$08.00+0 doi:10.1128/JVI.01702-06
Copyright © 2007, American Society for Microbiology. All Rights Reserved.

Severe Acute Respiratory Syndrome Coronavirus Infection of Mice Transgenic for the Human Angiotensin-Converting Enzyme 2 Virus Receptor▽

Chien-Te K. Tseng,[1,3]* Cheng Huang,[1] Patrick Newman,[2] Nan Wang,[1] Krishna Narayanan,[1] Douglas M. Watts,[2,3] Shinji Makino,[1,3] Michelle M. Packard,[4] Sherif R. Zaki,[4] Teh-sheng Chan,[1] and Clarence J. Peters[1,2,3]

Departments of Microbiology and Immunology[1] and Pathology[2] and the Center of Biodefense and Emerging Infectious Disease,[3] University of Texas Medical Branch, Galveston, Texas, and Centers for Disease Control and Prevention, Atlanta, Georgia[4]

Received 7 August 2006/Accepted 10 November 2006

Animal models for severe acute respiratory syndrome (SARS) coronavirus infection of humans are needed to elucidate SARS pathogenesis and develop vaccines and antivirals. We developed transgenic mice expressing human angiotensin-converting enzyme 2, a functional receptor for the virus, under the regulation of a global promoter. A transgenic lineage, designated AC70, was among the best characterized against SARS coronavirus infection, showing weight loss and other clinical manifestations before reaching 100% mortality within 8 days after intranasal infection. High virus titers were detected in the lungs and brains of transgene-positive (Tg^+) mice on days 1 and 3 after infection. Inflammatory mediators were also detected in these tissues, coinciding with high levels of virus replication. Lower virus titers were also detected in other tissues, including blood. In contrast, infected transgene-negative (Tg^-) mice survived without showing any clinical illness. Pathologic examination suggests that the extensive involvement of the central nervous system likely contributed to the death of Tg^+ mice, even though viral pneumonia was present. Preliminary studies with mice of a second lineage, AC63, in which the transgene expression was considerably less abundant than that in the AC70 line, revealed that virus replication was largely restricted to the lungs but not the brain. Importantly, despite significant weight loss, infected Tg^+ AC63 mice eventually recovered from the illness without any mortality. The severity of the disease that developed in these transgenic mice—AC70 in particular—makes these mouse models valuable not only for evaluating the efficacy of antivirals and vaccines, but also for studying SARS coronavirus pathogenesis.

Severe acute respiratory syndrome (SARS) coronavirus (CoV) is a highly transmissible human pathogen, which emerged in late 2002 in southern China and spread to Asian and western hemisphere countries. The disease was successfully contained by July of 2003, following the application of intensive public health measures, but not before causing ~8,000 clinical cases with an ~10% case fatality and tremendous economic impact worldwide. The most likely hypothesis for the emergence of SARS-CoV is that the virus from the natural reservoir, presumably the Chinese horseshoe bat (*Rhinolophus sinicus*), adapted to infect civets, which were permissive, and resulted in an epidemic among civets, which were sold in the southern China food markets (19, 21). The virus then spread to humans and underwent further genetic adaptation, particularly to the spike protein, to become more efficiently transmissible among the human population (22, 35). It seems unlikely that this first emergence of SARS will be a unique event, because many viruses such as Ebola virus, Venezuelan equine encephalitis virus, and epidemic influenza viruses have all returned after a hiatus in transmission. Thus, the need for effective antiviral agents and vaccines would be essential should SARS reemerge in the future.

Animal models are crucial to understanding the pathogenesis of human SARS and evaluating the efficacy of antiviral drugs and vaccines. Several animal models for SARS have been proposed, namely nonhuman primates (i.e., macaques, African green monkeys, and marmosets), ferrets, hamsters, and mice, including young and aged BALB/c and C57BL/6 mice and types lacking components of the immune system (i.e., Stat1- and RAG1-knockout mice) (9, 18, 23, 31, 32, 36, 37). These animals were shown to be susceptible to SARS-CoV infection and showed viral replication, some degree of histopathology, and, occasionally, limited clinical illness. However, none exhibited consistent clinical illness or mortality. Additionally, all suffer from some disadvantages, including high cost, poor availability of reagents, and an immunological response profile to the infecting virus quite unlike that observed in the human disease. Aged mice, in keeping with elderly humans, have more pathology than do normal mice. However, a mild weight loss has been the only clinical manifestation in response to SARS-CoV infection. Stat1-deficient mice show more pronounced changes than do normal mice, but there is no mortality and the pathological changes are not typical of those found with human SARS.

The tropism of coronaviruses is determined primarily by the interaction of the spike (S) protein and the cellular receptors for the virus. Human angiotensin-converting en-

* Corresponding author. Mailing address: Department of Microbiology and Immunology, University of Texas Medical Branch, 301 University Boulevard, G-150 Keiller Building, Galveston, TX 77555-0609. Phone: (409) 772-0175. Fax: (409) 747-0762. E-mail: sktseng@utmb.edu.

▽ Published ahead of print on 15 November 2006.

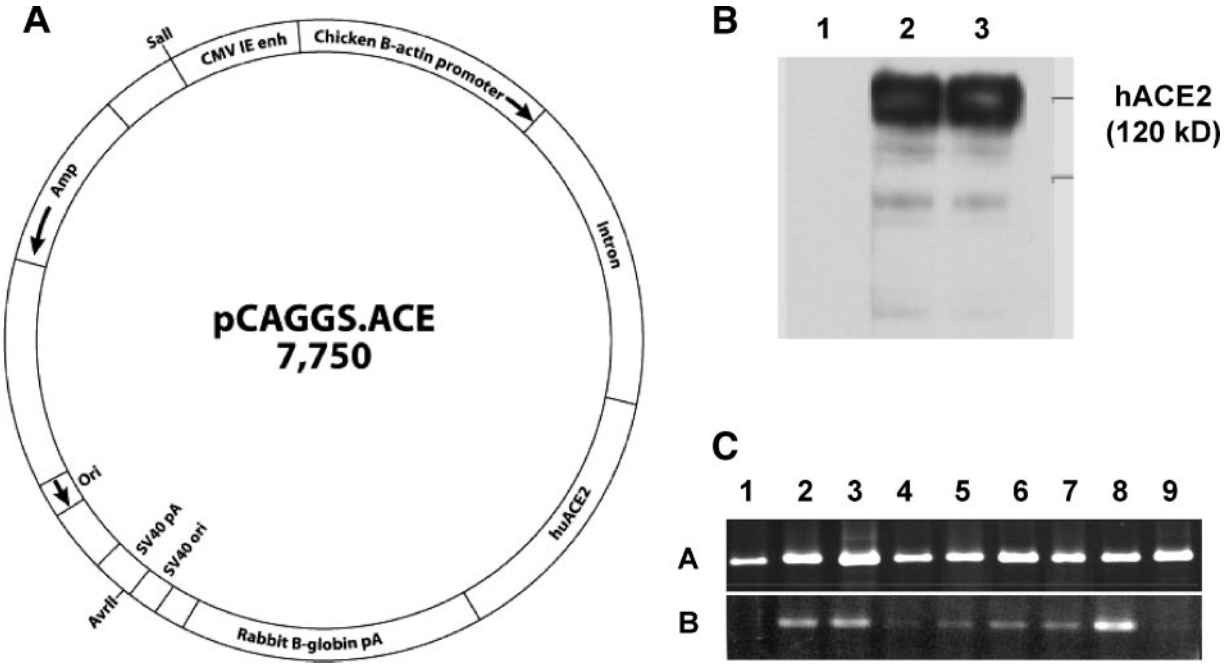

FIG. 1. Construction and characterization of hACE2 transgene. (A) Diagram of hACE2 expression cassette. The entire open reading frame of human ACE2 (hACE2) was amplified by RT-PCR using mRNAs extracted from a human colon cancer cell line, Caco-2. The resulting cDNA of hACE2 was inserted into the expression vector pCAGGS.MCS, downstream of the CAG promoter, as described in Materials and Methods. The resulting plasmid was named pCAGGS.ACE. CMV-IE enh, CMV-IE enhancer. (B) Western blot analysis of hACE2 expression in transfected human 293 cells. Cell extracts prepared from mock-transfected (lane 1) or pCAGGS.ACE-transfected (lanes 2 and 3) human 293 cells were subjected to Western blot analysis to verify transgene expression using monoclonal antibody against hACE2. (C) Tissue expression profile of hACE2 in the transgenic mouse lineages AC70 (A) and AC63 (B). DNA-free RNAs extracted from different organs of transgenic mice at 6 to 8 weeks of age were subjected to RT-PCR analysis to evaluate the expression of hACE2 mRNA. The RT-PCR products were analyzed on 2% agarose gel. Lanes 1 to 9 represent spleen, stomach, heart, muscle, brain, kidney, lungs, intestine, and liver, respectively. The data shown are representative of two independently conducted experiments.

zyme 2 (hACE2) has been identified as a major receptor for SARS-CoV. The spike protein of SARS-CoV has a much higher binding affinity to hACE2 than do those of mice, rats, and other animal species, which correlates with the much lower level of permissiveness of these animals to this virus (22). Thus, one strategy for establishing an economical and suitable animal model for SARS is to establish transgenic mouse lines expressing hACE2. We have generated five lineages of such a transgenic mouse, among which three die in response to SARS-CoV infection. Here, we present detailed information about the infectivity and tissue distribution of SARS-CoV, virus-associated histopathology, inflammatory responses, and the clinical manifestations in transgenic mice of the AC70 line, one of the three lineages that succumbed to an acute and fatal infection. We also present the data from the preliminary studies with transgenic AC63 mice, one of the nonlethal lineages, showing that despite of the onset of significant weight loss and other signs of illness, infected AC63 mice eventually recovered from the infection without any mortality. Importantly, in contrast to AC70 mice, in which both lungs and brains are the major sites of infection, virus replication in the AC63 mice is largely restricted to the lungs. Taken together, the severity of illness and/or the fatal outcome of these transgenic mouse lineages make them attractive models for the evaluation of the prophylactic and therapeutic efficacy of antiviral drugs and vaccines against SARS-CoV infection.

MATERIALS AND METHODS

Construction and expression of the hACE2 transgene. The cDNA coding for hACE2 was generated by reverse transcription-PCR (RT-PCR) amplification from a human colon carcinoma cell line, Caco2, which supported SARS-CoV replication (24). The resulting PCR product was cloned into the pSTblue-1 cloning vector (Novagen), and the entire region corresponding to the ACE2 gene was confirmed by sequencing (not shown). The cDNA fragment containing the ACE2 sequences was subsequently cloned into a eukaryotic expression vector, pCAGGS/MCS (a gift from Yoshihiro Kawaoka, University of Wisconsin at Madison), under the control of the CAG promoter, a composite promoter consisting of the cytomegalovirus immediate-early (CMV-IE) enhancer and the chicken β-actin promoter and containing the rabbit globin splicing and polyadenylation site. To verify the expression of hACE2, human embryonic kidney 293 cells were transfected with the resulting plasmid construct, designated pCAGGS-ACE2 (Fig. 1A), using Lipofectamine 2000 reagent (Invitrogen, Carlsbad, CA) per the manufacturer's protocols. Cell extracts were prepared 24 h after transfection, and the expression of hACE2 was examined by Western blot analysis using polyclonal antibody against hACE2 (R&D Systems).

Generation and characterization of transgenic mice. Transgenic mice expressing human ACE2 were generated by microinjecting the expression cassette, which was excised from pCAGGS-ACE2 by AvrII/SalI digestion and purified by agarose gel electrophoresis, into pronuclei of zygotes from the intercross of (C57BL/6J × C3H/HeJ) F_1 parents. Transgenic mice were initially identified by PCR of genomic DNA with hACE2-specific primers: forward, 5′-AGGATGTG CGAGTGGCTA-3′, and reverse, 5′-AGGGCCATCAGGATGTCC-3′, amplifying a transgene-specific fragment of 195 bp (data not shown). A total of five lineages, expressing different levels of hACE2 in the tail biopsies, were established. Two of the lineages, designated AC70 and AC63, respectively, were further investigated with regard to the tissue distribution of hACE2 transgene expression by RT-PCR with the same hACE2-specific primers as described above, followed by agarose gel analysis of PCR products.

Virus and cells. The Urbani strain of SARS-CoV at the Vero 2nd passage level, kindly provided to us by T. G. Ksiazek, Centers for Disease Control and Prevention (Atlanta, GA), was used throughout this study. Vero E6 cells (American Type Culture Collection) were used to grow virus stocks and as indicator cells for the virus infectivity assay. Stocks of SARS-CoV were prepared by passaging them twice in Vero E6 cells at a low multiplicity of infection, 0.001, generating cell-free viral stocks with titers expressed as a 50% tissue culture infectious dose ($TCID_{50}$)/ml of sample (typically, 1×10^8 $TCID_{50}$/ml), aliquoted, and stored at −80°C. All experiments involving infectious virus were conducted at the University of Texas Medical Branch (Galveston, TX) in approved biosafety level 3 laboratories and animal facilities, with routine medical monitoring of staff.

Viral infection and morbidity and mortality studies of infected mice. All animal experiments were carried out in accordance with animal protocols approved by the IACUC committee at University of Texas Medical Branch. Mice used in this study were backcrossed two to three times onto either a C57BL/6 or BALB/c background. We did not observe any difference with regard to the susceptibility to SARS-CoV among mice derived from the different genetic backgrounds. Briefly, anesthetized transgenic mice and their nontransgenic littermates at the ages of 8 to 20 weeks were inoculated via the intranasal (i.n.) route with 10^3 or 2×10^5 $TCID_{50}$ of virus in 40 μl of saline. Animals were weighed and observed daily for sign of illness and mortality. In some experiments, infected mice were sacrificed at indicated time intervals after inoculation to obtain selected tissue specimens to define the viral distribution by viral titration in Vero E6 cells and by quantitative RT-PCR assay and for histopathology analysis.

Assessment of tissue distribution of SARS-CoV in infected animals. In addition to blood, throat and nasal turbinate washes, and urine, solid tissue specimens (i.e., the lungs, brain, heart, liver, kidney, spleen, mesenteric lymph nodes [mLNs], and small and large bowels) and feces were weighed and homogenized in a phosphate-buffered saline [PBS]–10% fetal calf serum solution using the TissueLyser-QIAGEN (Retsch, Haan, Germany) to yield 10% tissue–PBS suspensions. These suspensions were clarified by centrifugation and subjected to virus titration with the standard infectivity assay using Vero E6 cells. The virus titer of individual samples was expressed as $TCID_{50}$ per ml or per g of sample.

Q-RT-PCR for SARS-CoV subgenomic RNAs. Total RNA was isolated from tissues of infected mice at indicated time intervals after infection using an RNeasy Mini kit (QIAGEN Sciences). Contaminating genomic DNA was removed upon digestion with DNase I during the extraction procedure. Resulting RNA specimens were subjected to one-step quantitative real-time RT-PCR (Q-RT-PCR) analysis to assess the expression of SARS-CoV-specific subgenomic mRNA 1 and mRNA 5, according to the methodologies established in our laboratories (40, 41). The following primers and detection probes were used: for RNA 5, forward, 5′-AGGTTTCCTATTCCTAGCCTGGATT-3′, and reverse, 5′-AGAGCCAGAGGAAAACAAGCTTTAT-3′, with the sequence of ACCTGTTCCGATTAGAATAG as a detection probe; and for RNA 1, forward, 5′-TCTGCGGATGCATCAACGT-3′, and reverse, 5′-TGTAAGACGGGCTG CACTT-3′, with the sequence of CCGCAAACCCGTTTAAA as a detection probe—all of these were derived by using the Assays-by-Design software (Applied Biosystems). The selected primer set and Taq-Man probe for 18S rRNA were used as the endogenous control. Briefly, 80 ng RNA was transferred to separate tubes for amplification of the target genes and endogenous control (18S rRNA), respectively, by using a TaqMan one-step RT-PCR master mix reagent kit. The cycling parameters for one-step RT-PCR were as follows: reverse transcription at 48°C for 30 min, AmpliTaq activation at 95°C for 10 min, denaturation at 95°C for 15 s, and annealing/extension at 60°C for 1 min. A total of 40 cycles were performed on an ABI PRISM 7000 real-time thermocycler (Applied Biosystems) following the manufacturer's instructions. DNA fragments encoding target genes were amplified in triplicate and relative mRNA levels for each sample were calculated as follows: $\Delta C_T = C_T$ of target genes $- C_T$ of 18S rRNA. The relative abundance of the RNA for hACE2 or for SARS-CoV was expressed as $2^{-(\Delta C_T \text{ infected} - \Delta C_T \text{ mock})}$.

Histology and IHC. Multiple tissues obtained from necropsy were fixed in 10% buffered formalin for 72 h, transferred to 70% ethanol, and later paraffin embedded. Histopathologic evaluation was performed on deparaffinized sections stained by routine hematoxylin-and-eosin staining. Immunohistochemical (IHC) testing for SARS-CoV was applied using a previously described colorimetric indirect immunoalkaline phosphatase method (36) with a rabbit anti-SARS-CoV nucleocapsid protein antibody (Imgenex, catalog no. IMG-548). The goat anti-human ACE2 antibody (R&D Systems, catalog no. AF933) was used to evaluate the distribution of hACE2 expression in transgenic mice by IHC. Normal mouse and goat sera were used as negative antibody controls. Primary antibodies were detected with either biotinylated swine anti-rabbit immunoglobulin (DAKO catalog no. E0353) or rabbit anti-goat immunoglobulin (KPL catalog no. 16-13-06) secondary antibodies. Visualization was then achieved by incubation with streptavidin-alkaline phosphatase and naphthol-fast red substrate (DAKO) and counterstaining with Mayer's hematoxylin (Fisher Scientific).

Measurement of inflammatory cytokines and chemokines. Inactivated (γ irradiation) tissue homogenates were used to define cytokine profiles by Bio-Plex cytometric bead array (Bio-Rad, Hercules, CA) analysis according to the manufacturer's recommendation. This technology was used to simultaneously quantify up to 23 inflammatory mediators (see Results for the list).

Statistical analysis. Viral titers and the contents of inflammatory cytokines and chemokines were compared between groups of mice and tested for significance of differences by Student's *t* test.

RESULTS

Generation of hACE2 transgenic mice and detection of transgene expression. To verify hACE2 expression of pCAGGS-ACE2 plasmid (Fig. 1A), human embryonic 293 cells were transfected with this plasmid and cell extracts were prepared at 24 h posttransfection. The expression of ACE2 was examined by Western blot analysis using specific antibody to ACE2. As shown in Fig. 1B, an abundant expression of ACE2 of about 120 kDa was readily detectable in transfected cells, whereas this signal could not be detected in untransfected cells.

Microinjection of this ACE2-expressing cassette DNA into F_2 zygotes from F_1 mice (C57BL/6J × C3H/HeJ) resulted in five viable founder animals, designated AC-12, -22, -50, -63, and -70, respectively. These founders were backcrossed to C56BL/6 or BALB/c mice. The hACE2 transgene in the litters was monitored by PCR, showing that all the founders appeared to transmit the transgene to their progenies (data not shown). The hACE2 expression in different organs of AC70 and AC63 transgenic lineages was subsequently evaluated by RT-PCR. As shown in Fig. 1C, the ACE2 transgene was ubiquitously expressed in both AC70 and AC63 lines, with AC70 at a much higher level than AC63.

SARS-CoV-induced morbidity and mortality in Tg^+ AC70 mice. High levels of ACE2 expression in AC70 mice prompted us to investigate the outcome of SARS-CoV infection in this particular lineage. The susceptibility of transgene-positive (Tg^+) and their transgene-negative (Tg^-) littermates, ranging from 2 to 6 months of age, was determined in a pilot study by inoculating mice with either 2×10^5 or 10^3 $TCID_{50}$ of SARS-CoV per mouse, via the i.n. route. All infected Tg^+ mice, but not their age-matched Tg^- littermates, developed an acute wasting syndrome and died within 4 to 8 days postinfection (p.i.) with either dose. Thus, the lower dosage, i.e., 10^3 $TCID_{50}$, was adopted in the subsequent studies to verify the pathogenesis of SARS-CoV infection.

For the next experiment, we inoculated (i.n.) Tg^+ and Tg^- AC70 mice, 10 animals in each group, with SARS-CoV. Infected mice were observed for signs of clinical illness daily. Early clinical manifestations of infected Tg^+ mice included ruffled fur, lethargy, and rapid, shallow breathing, accompanied by persistent weight loss, which could reach up to 35 to 40% in some mice (Fig. 2A). This relentless weight loss may have been caused by wastage, which is associated with many viral diseases and aggravated by inappetence, due to the decreased and apparently uncontrolled directional movement. There were no seizures or obvious paralysis, but the mice died after a period of immobility lasting 1 to 3 days. Mortality began

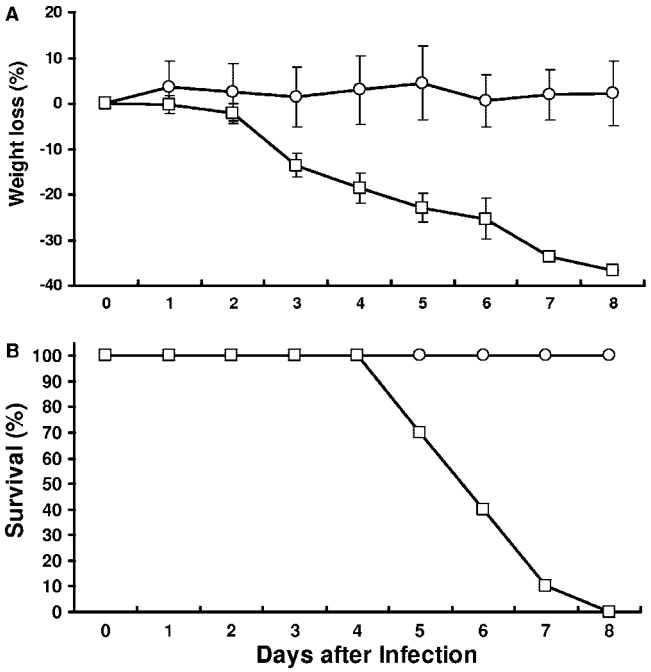

FIG. 2. Weight loss and survival rate of SARS-CoV-infected AC70 Tg^+ mice and their Tg^- littermates. Tg^+ and Tg^- mice at 8 to 12 weeks of age were i.n. inoculated with 1×10^3 $TCID_{50}$ of SARS-CoV (Urbani strain) in 40 μl saline. Body weights (A) and accumulated mortality (B) of infected Tg^+ (□) and Tg^- (○) mice were measured and recorded on a daily basis. Weight changes were expressed as the mean percent changes in infected animals ($n = 10$ per group, including those who died) relative to the initial weights at day 0. Error bars represent standard errors.

on day 4 p.i. and reached 100% by day 8 p.i. (Fig. 2B). All of the infected Tg^- mice continued to thrive throughout the entire course of infection without any significant weight loss or other clinical manifestations, findings which correlated with previous reports of normal mice (9, 36).

Distribution of SARS-CoV in tissues of infected AC70 mice. We next investigated the kinetics and tissue distribution of infectious virus by inoculating (i.n.) age-matched Tg^+ and Tg^- mice (15 per group). Three mice in each group were sacrificed at daily intervals, except for the fifth day, at which only one Tg^+ mouse survived the infection, and the titers of infectious virus in various tissues were determined in Vero E6 cells, as described in Materials and Methods. Among the tissues examined, the lungs and the brain were the major sites of viral replication, particularly in Tg^+ mice. As shown in Fig. 3A, maximum viral titers were detected in the lungs within 1 to 2 days p.i., with a median of $10^{8.5}$ and $10^{6.5}$ $TCID_{50}$/g of tissue for Tg^+ and Tg^- mice, respectively. Although the viral titers gradually decreased thereafter in the lungs of both strains of mice, relatively higher virus titers were recovered from Tg^+ mice than from their Tg^- littermates during the entire course of infection.

Viral replication was also detected in the brain of infected mice, with strikingly different kinetics from that of the lungs. A low titer of the virus was first detected in the brain of the Tg^+ mouse on day 2 p.i. Thereafter, virus replication proceeded rapidly and reached a median of more than 10^8 $TCID_{50}$/g at day 3 p.i. (Fig. 3B). In contrast to the decreasing trend of infectious virus over time in the lungs, viral titers remained high in the brain, starting at day 3 until the death of the host. Although infectious virus was also detectable in the brain of some Tg^- mice at day 3 p.i., the titers of virus were significantly lower ($P < 0.01$) than those of Tg^+ mice. The kinetics of SARS-CoV replication in both tissues was confirmed by Q-RT-PCR analysis targeting SARS-CoV-specific subgenomic mRNA5 (Fig. 3C and D) and mRNA 1 (data not shown).

A low, but detectable, level of infectious virus, usually less than 10^4 $TCID_{50}$/ml or g was also detected in 8/12 Tg^+ and 4/15 Tg^- nasal washes, 3/12 Tg^+ and 1/15 Tg^- liver specimens, and 1/12 Tg^+ large bowels collected from infected animals at various time points. However, we were unable to detect any infectious virus in throat swabs, blood, heart, spleen, mLNs, kidneys, urine, or feces by the infectivity assay, in which the detection limit was greater than 10^3 $TCID_{50}$/ml or 10^3 $TCID_{50}$/g of tissue.

To investigate whether the virus spread to the brain was unique to the i.n. route of infection, we challenged AC70 mice with 10^3 $TCID_{50}$ of virus through the intraperitoneal (i.p.) route. While infected Tg^- mice appeared to be healthy, Tg^+ animals started to show signs of illness at day 4 p.i. and were thus sacrificed, along with four apparently "healthy" Tg^- littermates, to determine the viral titers in the lungs and the brain. As shown in Fig. 4, all infected Tg^+ mice exhibited high viral titers in the brains, whereas only two of the four infected Tg^- mice had infectious virus in this organ at a significantly lower titer ($P < 0.01$). Interestingly, we were unable to recover any infectious virus from the lungs of either strain of mice. These results clearly indicated that the dissemination of infectious SARS-CoV to the brain is independent of the route of the infection.

Although we were unable to detect infectious virus in the circulation in our earlier studies, the extremely high recovery of infectious virus from the brains of i.p.-challenged Tg^+ mice prompted us to reevaluate the viremic status of infected animals. We inoculated (i.n.) five Tg^+ mice with 10^3 $TCID_{50}$ of the virus. To increase the sensitivity of detection, instead of using the blood specimens that were diluted (1:10) and a small portion of the spleen in our earlier studies, we collected undiluted blood specimens and the whole spleens of infected animals at day 2 p.i. for the infectivity assays. With this improved method, we were able to detect infectious virus from both tissues in all of the infected animals at titers ranging from 10^2 to $10^{2.5}$ $TCID_{50}$, a titer that was below the limit of detection in our earlier studies, suggesting that a low-level of viremia did exist in infected Tg^+ mice.

Histopathology and immunohistochemistry. The histopathology of SARS is characterized by an interstitial pneumonitis, diffuse alveolar damage, with extensive alveolar collapse, and filling of remaining alveoli with fluid and desquamated epithelial cells (17, 26, 34). Histological examination of infected AC70 mice at day 2 p.i. revealed a moderate interstitial pneumonitis with focal thickening of alveolar wall and filling of alveolar sacs and small airways with cellular debris and macrophage-like cells. IHC staining showed that SARS-CoV antigen was readily detected in the bronchial epithelial cells and in association with the inflammatory infiltrate in the pulmonary interstitium of infected Tg^+ mice (Fig. 5A and B). This detec-

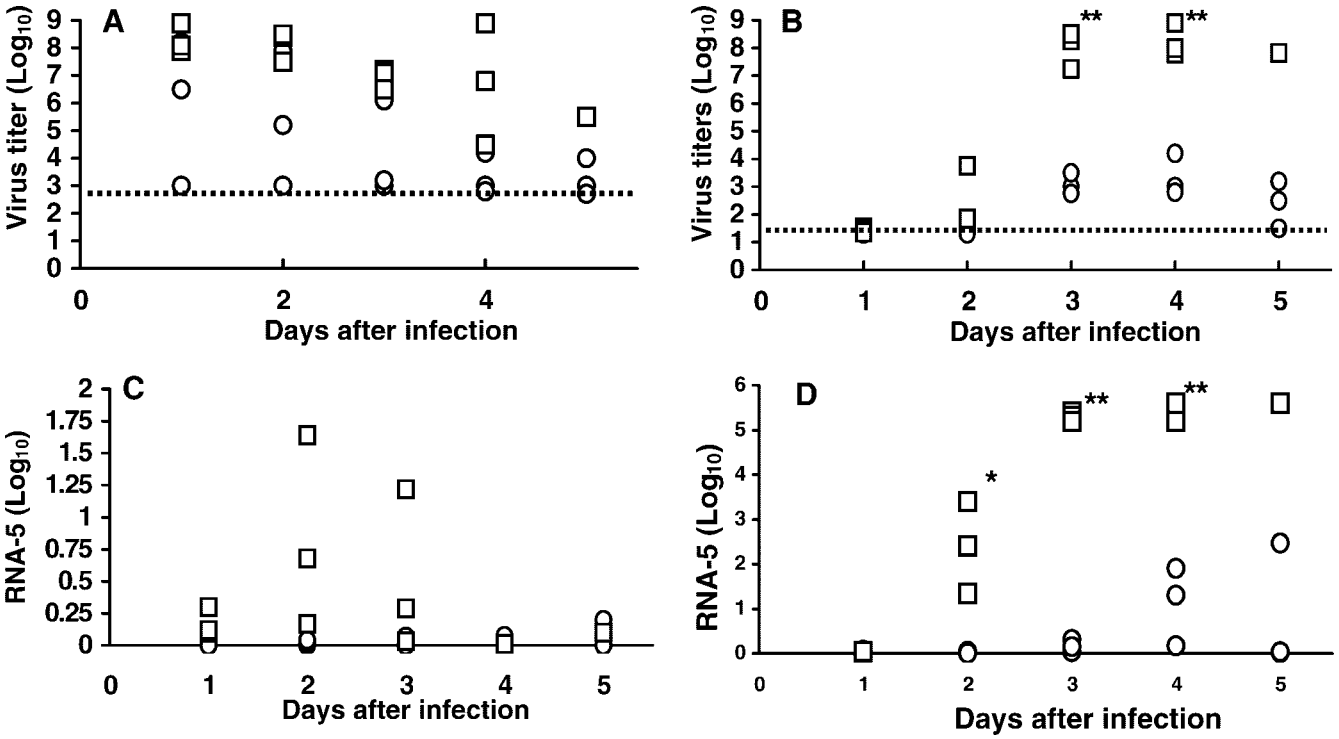

FIG. 3. Kinetics of SARS-CoV replication in the lungs and brain of infected mice. Tg^+ mice (□) and their Tg^- littermates (○) ($n = 15$ per group) were inoculated (i.n.) with 10^5 $TCID_{50}$ of SARS-CoV in 40 μl saline. Three animals in each group were sacrificed daily, and virus titers in the lungs and brains were assessed by using both the standard $TCID_{50}$ assay in Vero E6 cells and quantitative RT-PCR analysis, as described in Materials and Methods. The titers of infectious virus in the lungs (A) and brain (B) were calculated and expressed as $\log_{10}$ $TCID_{50}$ virus per gram of tissue, whereas the relative copy numbers of SARS-CoV mRNA 5 (encoding M protein) of the lung (C) and brain (D) specimens as determined by Q-RT-PCR after normalization against 18S rRNA as the internal control were plotted (by the C_T method). The average of mRNA 5 signals in duplicated samples of individual specimens is depicted. *, $P < 0.05$, and **, $P < 0.01$, by Student's t test, comparing Tg^+ and Tg^- mice.

tion of SARS-CoV antigen was specific, since staining of the lung tissues obtained from the same infected animals with irrelevant mouse antibodies was negative for the viral antigen (Fig. 5C). Infected bronchial epithelial cells showed cytoplasmic swelling and blebbing and were surrounded by moderate inflammatory mononuclear infiltrates. Cellular debris associated with abundant viral antigen was seen within the bronchial lumen (Fig. 5D and E). Although the SARS-CoV was also detected in the lungs of infected Tg^- mice, the frequencies of infected cells and viral antigen were much lower than those of Tg^+ mice (data not shown). No extrapulmonary SARS-CoV antigens were detected by IHC in Tg^- mice. SARS-CoV antigen was also detected in vascular smooth muscle and ganglion cells in the lungs of Tg^+ mice by day 3 (Fig. 5F and G). SARS-CoV antigen present in the smooth muscle of blood vessels was associated with a mild to moderate vasculitis (Fig. 5F).

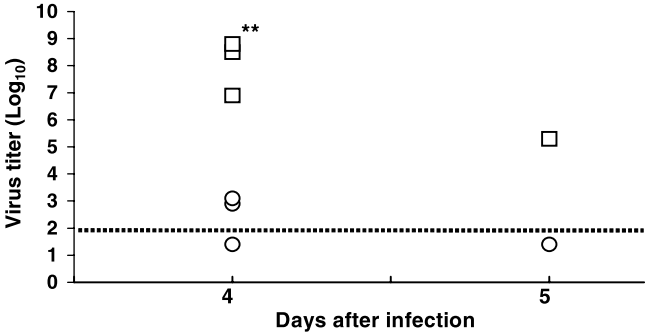

FIG. 4. SARS-CoV replicates in the brains of mice following intraperitoneal inoculation. Tg^+ (□) and Tg^- (○) mice (four in each group) were inoculated with 10^3 $TCID_{50}$ of SARS-CoV. Tg^+ mice started to show signs of illness at day 4. Three sick Tg^+ animals, along with three apparently healthy Tg^- counterparts, were sacrificed at day 4 ($n = 3$), and the remaining mouse from each group was sacrificed at day 5 to titrate infectious virus in the brains. The infectious virus titer of individual mice is expressed as the $\log_{10}$ $TCID_{50}$ per gram of tissue. **, $P < 0.01$ by Student's t test, comparing Tg^+ and aged-matched Tg^- mice.

High levels of SARS-CoV antigen expression were also detected at days 3 and 4 p.i. in abundant neurons and glial cells of the central nervous system (CNS) of infected Tg^+ mice (Fig. 5H and I), consistent with high titers of the virus in the brain at this stage. However, no necrosis or inflammatory reaction could be seen in association with the presence of SARS-CoV antigen in the CNS. Additionally, viral antigen was detected in the gastrointestinal (GI) tracts of Tg^+ mice at day 6 p.i., even though infectious virus was rarely recovered in this tissue. Within the GI tract, virus antigen was restricted to the subserosal ganglia (Fig. 5J) and smooth muscle of the intestinal wall (data not shown).

The expression of hACE2 antigen was detected in the lungs, kidneys, liver, heart, skeletal muscle, spleen, LN, pancreas,

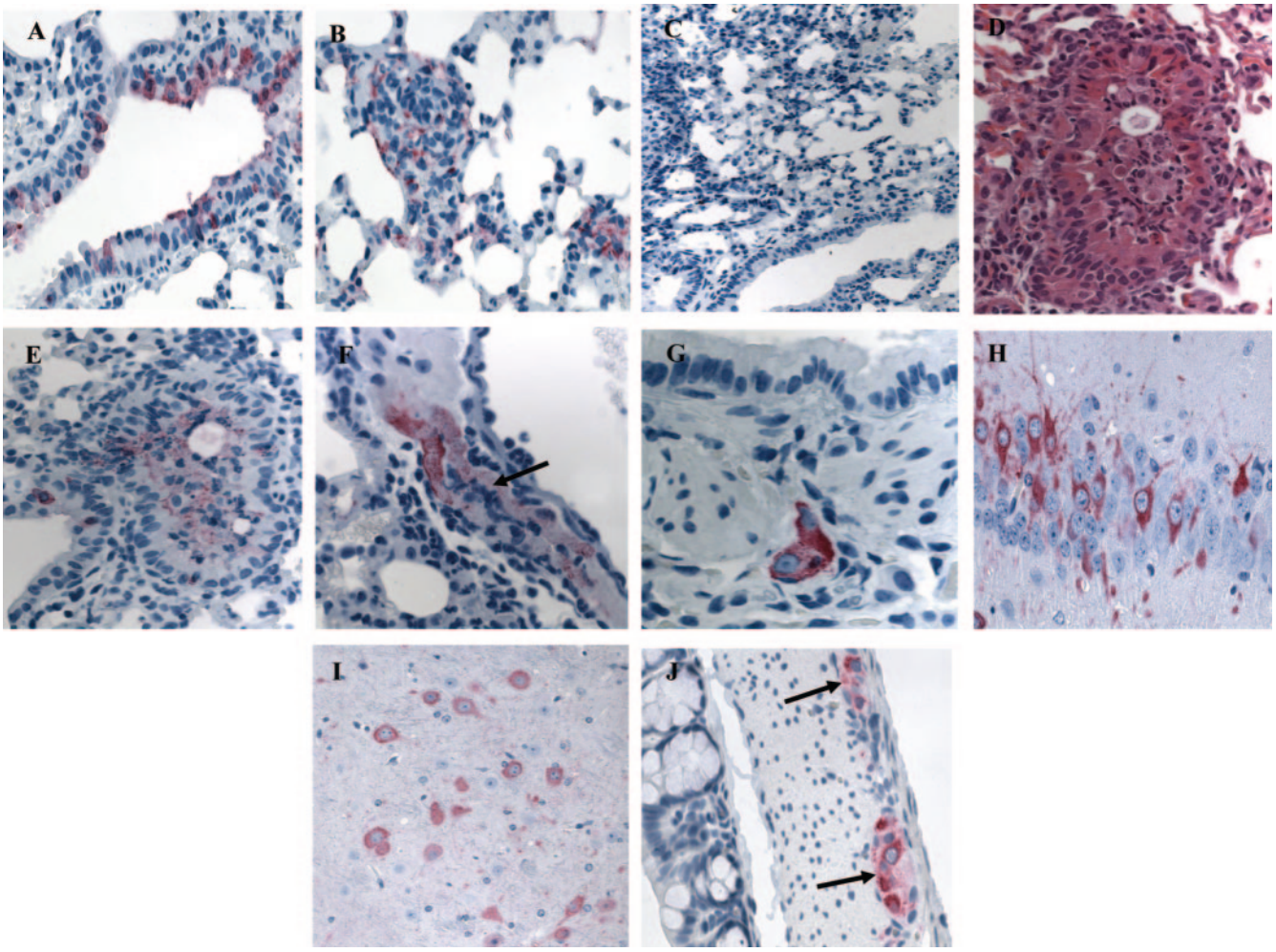

FIG. 5. Histopathology and immunohistochemical analysis of SARS-CoV antigen expression in the lungs, brain, and GI tract of Tg^+ mice after infection (i.n.). Paraffin-embedded lung (A to G), brain (H and I), and GI tract (J) sections of infected Tg^+ mice were analyzed for the pathology and expression of the nucleocapsid protein of SARS-CoV by the methodologies described in Materials and Methods. SARS-CoV antigen (red) was readily detectable in the cytoplasm of epithelial cells of the bronchial lining (A) and pulmonary interstitium (B) at day 2. No staining was seen in the same Tg^+ mouse when immunohistochemistry was performed with normal mouse ascites fluid (C). Shown are serial sections (hematoxylin and eosin in panel D and IHC in panel E) of a bronchus showing intraluminal macrophages and cellular debris in association with viral antigen. (F) Inflammatory cellular infiltrates (arrow) within smooth muscle of a pulmonary blood vessel associated with SARS-CoV antigen. (G) SARS-CoV immunostaining of a subepithelial ganglion cell in the lung at day 2. Extensive SARS-CoV antigen expression was first detected on day 3 in large numbers of morphologically intact neuronal and glial cells in the CNS (H and I). In the GI tract, the expression of SARS-CoV antigen in ganglia within the subserosal layer (arrow) was detected first at day 4 (J). Magnifications: A to F, H, and J, ×100; G, ×158; I, ×50. Staining: panels A to C and E to J, IHC with naphthol red and hematoxylin counterstaining; panel D, hematoxylin and eosin.

gastrointestinal smooth muscle and ganglia, vascular endothelium, adrenal, and CNS of Tg^+ mice. In the IHC assay used in this study, staining of hACE2 was specific for the human protein; no such expression was detected in Tg^- mice, and no staining was seen using normal goat serum as a negative control (data not shown). Although two-color staining was not performed to colocalize hACE2 and viral antigen expression, we noticed that in the lungs and GI tract, the viral distribution correlated well with the pattern of expression observed for hACE2. In the lungs of Tg^+ mice, hACE2 was detected primarily in the pneumocytes, vascular smooth muscle, and ganglion cells (Fig. 6A and B). Expression was found focally in the muscularis and subserosal ganglia of the GI system, in similar areas to those where SARS-CoV antigen was present (Fig. 6H). In comparison, in the CNS the distribution of viral antigen and hACE2 was significantly different. High levels of hACE2 expression were detected in choroid, ventricular lining, and vascular endothelial cells, while only rare neurons and glial cells showed minimal expression of hACE2 (Fig. 6C to G). However, intense staining of SARS-CoV was only detected in neuron and glial cells (above), suggesting that not all of the hACE2-expressing cells are susceptible to the infection.

SARS-CoV-induced cytokines and chemokines in the lungs and brains of mice. The mechanism of SARS-associated lung pathology remains unknown. However, pathological studies with postmortem specimens of SARS patients reveal diffuse alveolar damage (DAD), hemophagocytosis, and prominent infiltration of activated macrophages in the lungs, which sug-

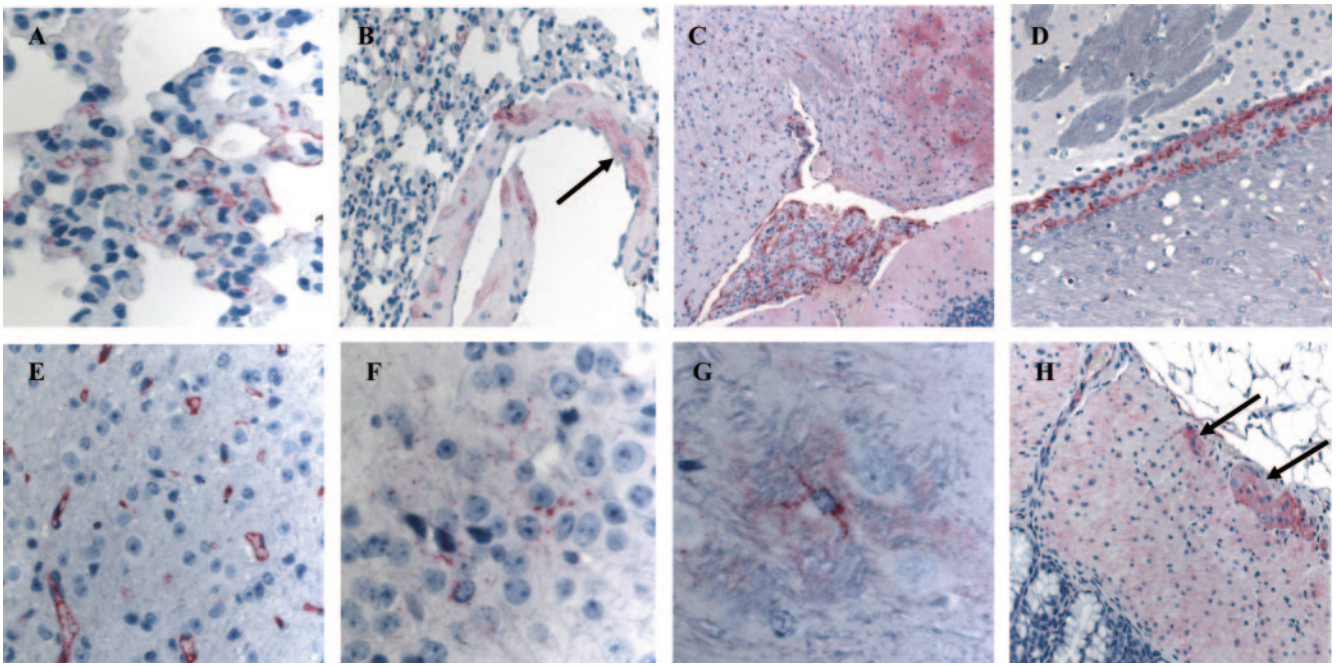

FIG. 6. Expression of hACE2 in the lungs, brain, and GI tract of Tg^+ mice. The paraffin-embedded sections of the lungs, brains, and GI tract were used to evaluate the expression of the hACE2 by IHC. The hACE2 antigen (red) was readily detectable primarily in the pneumocytes (A) and vascular smooth muscle in the lung (B, arrow). The hACE2 expression in the brain was also abundantly associated with choroid (C), ventricular lining (D), vascular endothelial cells (E), and patches of neuronal and glial elements (F and G). Finally, hACE2 was also found in the epithelial lining, muscularis layer, and ganglia of the GI system (H, arrow). Magnification: panels A, F, and G, ×158; panels B, D, and H, ×50; panel C, ×25; and panel E, ×100.

gest that an intense and unregulated inflammatory response within the lungs may be partially responsible for the pathogenesis of human SARS-CoV infection (26).

The severity of the disease developed in Tg^+ mice in response to SARS-CoV infection prompted us to study the host responses by measuring the contents of various inflammatory mediators in the lungs and brain, two of the most affected tissues. As shown in Fig. 7, among 23 inflammatory mediators measured, we were able to detect negligible levels of inflammatory cytokines in the lungs of infected Tg^- mice over time, compared to the levels in uninfected controls, suggesting that SARS-CoV infection failed to induce cytokine production in Tg^- mice. In contrast, elevated levels of interleukin-1β (IL-1β), IL-12_{p40}, IL-12_{p70}, CXCL1 (KC), RANTES, and MCP-1 expression were readily detected in the lungs of Tg^+ mice in at least one time point during the first 3 days of the infection (Fig. 7). The SARS-CoV-induced inflammatory response in the brain was similarly evaluated. There was no significant expression of inflammatory mediators in infected Tg^+ and Tg^- mice on both day 1 and day 2 (data not shown). However, highly elevated levels of IL-6, IL-12_{p40}, granulocyte colony-stimulating factor (G-CSF), CXCL1 (KC), MIP-1α, and MCP-1 were detected at day 3 in the brains of Tg^+ mice, but not their Tg^- littermates (Table 1). Additionally, the secretion of IL-1α, IL-1β, granulocyte-macrophage CSF (GM-CSF), IL-12_{p70}, and RANTES was increased to various extents in the brain of the Tg^+ mouse. Other inflammatory mediators, such as IL-2, IL-3, IL-4, IL-5, IL-9, IL-10, IL-13, IL-17, gamma interferon (IFN-γ), and tumor necrosis factor alpha (TNF-α), were not significantly induced. Taken together, these results clearly demonstrate that Tg^+ mice, which had much higher levels of SARS-CoV replication in the lungs and brain than their Tg^- littermates, as shown in Fig. 3, could promptly elicit a strong inflammatory cytokine reaction to acute SARS-CoV infection. Importantly, this acute inflammatory response occurred later and more intensely in the brain than in the lungs, consistent with the level of virus replication in respective organs.

SARS-CoV infection in transgenic AC63 mice. The susceptibility of Tg^+ AC63 mice to SARS-CoV infection was initially evaluated by using the same challenge strategy: i.e., 10^3 $TCID_{50}$ of SARS-CoV via the i.n. route. The Tg^+ AC63 mice were more susceptible to SARS-CoV infection than their Tg^- littermates, as evidenced by a moderate but progressive weight loss until day 8 (Fig. 8A). However, in contrast to the uniform mortality of infected Tg^+ AC70 mice, all infected AC63 mice eventually recovered from the weight loss without any death. We next investigated the tissue distribution of infectious virus and whether inoculation with a higher dose of virus could result in a fatal outcome. We inoculated (i.n.) both AC63 mice and control littermates (10 of each) with 10^6 $TCID_{50}$ of virus. To quantify the viral loads in the lungs and brain, five and three mice from each group were sacrificed at days 3 and 8, respectively. The remaining animals were kept to assess morbidity and mortality. Infected Tg^+, but not Tg^-, mice started to show an progressive weight loss, along with other clinical manifestations, between day 3 and day 4. As shown in Fig. 8B, Tg^+ mice appeared to be more susceptible to SARS-CoV infection than their Tg^- littermates, as evidenced by a much higher titer of infectious virus in the lungs. Additionally, four out of five Tg^+ mice had high virus titers in the lungs, whereas only two

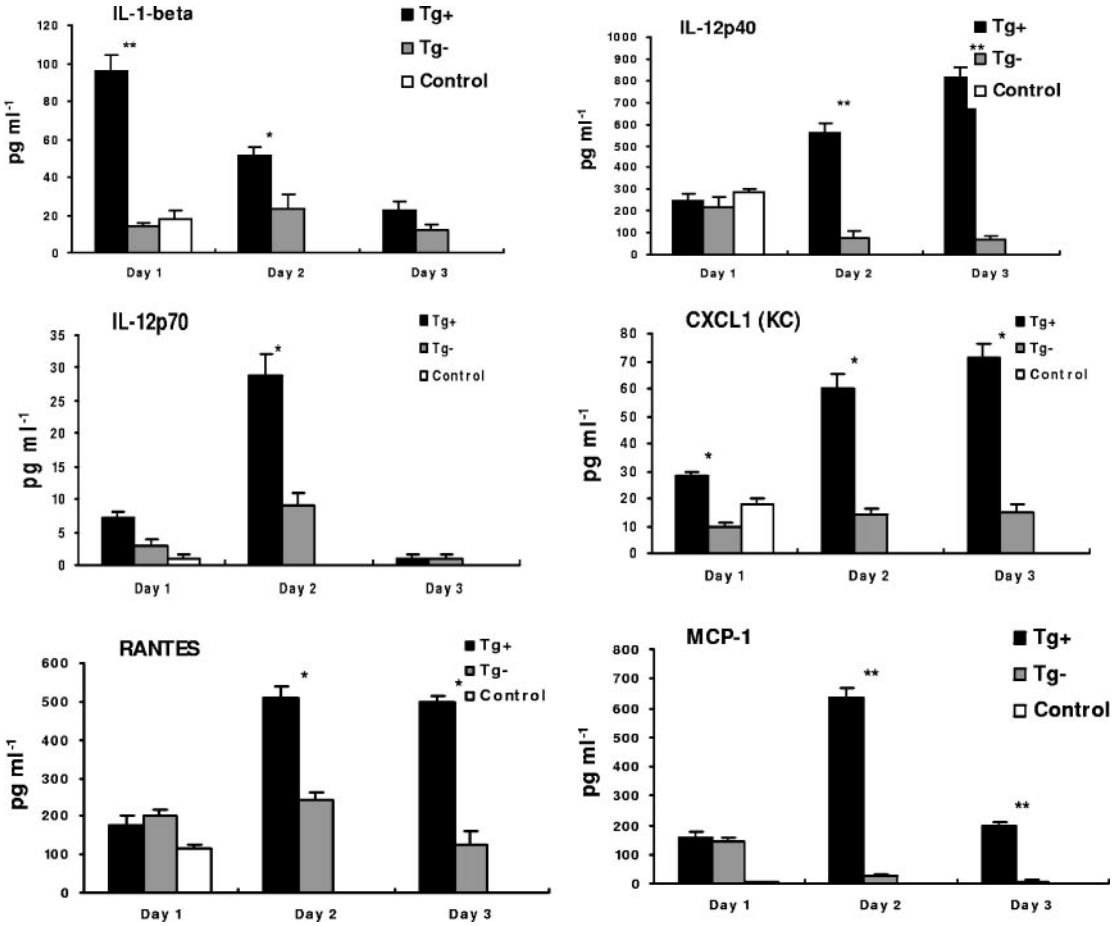

FIG. 7. Expression of pulmonary cytokines and chemokines in infected mice. Lung homogenates derived from mice at indicated time intervals after infection (i.n.) were subjected to Bio-Plex analysis for assessment of the concentrations of cytokines and chemokines. Among 23 inflammatory mediators tested, the expression of IL-1β, IL-12_{p40}, CXCL1/KC, RANTES, MCP-1, and IL-12_{p70} was elevated in infected Tg^+, but not Tg^-, mice. Duplicate samples of individual specimens were assayed. The data shown are the mean ± standard error of infected animals ($n = 3$) at indicated time points. *, $P < 0.05$, and **, $P < 0.01$, by Student's t test, comparing Tg^+ mice with aged-matched Tg^- controls.

TABLE 1. SARS-CoV-induced production of cytokines and chemokines in the brains of infected Tg^+ versus Tg^- mice

Inflammatory mediator	Cytokine or chemokine concn (pg/ml) in mouse brain[a]:	
	Tg^-	Tg^+
IL-6	3.2 ± 1	328 ± 40**
IL-12_{p40}	17 ± 2	2,500 ± 850**
G-CSF	2.6 ± 1	523 ± 58**
KC	25 ± 4	466 ± 75**
MIP-1a	ND	311 ± 35**
MCP-1	ND	904 ± 210**
IL-1α	7.5 ± 1	27 ± 4*
IL-1β	0.8 ± 0.5	31.4 ± 8
GM-CSF	2.5 ± 1	11 ± 2
IL-12_{p70}	12 ± 2	35 ± 5
RANTES	10.5 ± 3	55 ± 7*

[a] Homogenates of the brains harvested from each strain of mouse ($n = 3$) at the 3rd day postinfection were used to measure the concentrations of various cytokines and chemokines by the Bio-Plex analysis. Duplicate samples of individual specimens were assayed. ND, not detectable. Data are presented as the mean ± standard deviation of duplicate samples. *, $P < 0.05$, and **, $P < 0.01$, by Student's t test, compared with aged-matched Tg^- controls.

had low-to-moderate titers in the brain at day 3. Infectious virus was no longer detectable in the lungs at day 8, even though one animal still had detectable virus in the brain. Remarkably, despite the severity of the illness, as evidenced by the profound weight loss, the remaining animals started to show signs of recovery between day 8 and day 9, regained some of the lost weight in 1 week thereafter (Fig. 8C), and recovered completely in the ensuing 1 month when the experiment was terminated.

DISCUSSION

Animal models for SARS in well-characterized species that consistently reveal signs of illness, pathological findings, and mortality are highly desirable not only for studying pathogenesis, but also for evaluating the safety and efficacy of antiviral therapeutics and vaccine candidates against SARS-CoV infection. In this study, we developed a small animal model for SARS using transgenic mice expressing hACE2, the major cellular receptor for SARS-CoV (20). Not only could this transgenic mouse model support more robust viral growth than its nontransgenic littermates, but it also manifests respiratory

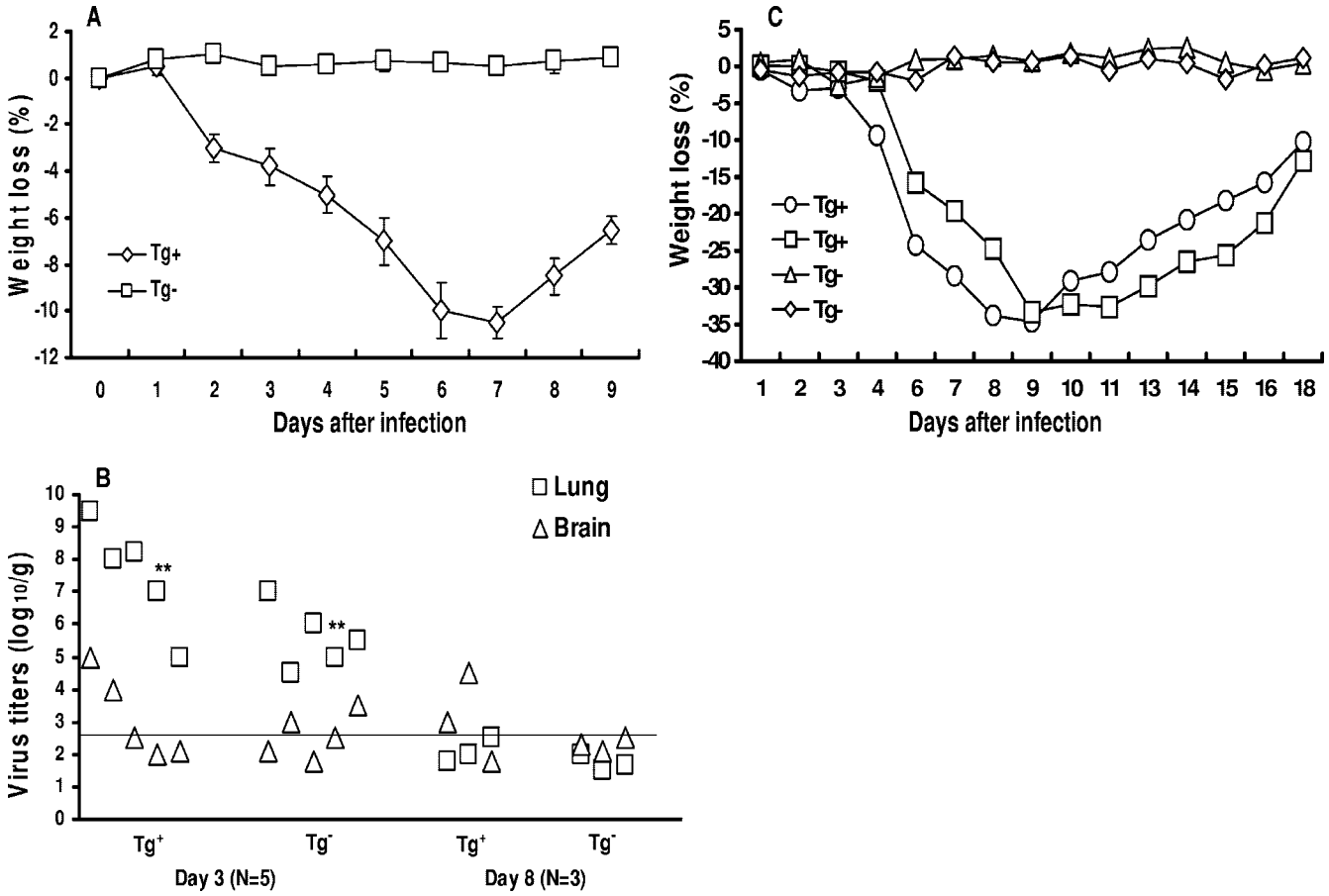

FIG. 8. Outcome in SARS-CoV-infected mice of the AC63 line. For the first experiment, Tg^+ and Tg^- mice of the AC63 line ($n = 10$ each) were inoculated (i.n.) with 10^3 $TCID_{50}$ of SARS-CoV, and the weight changes were recorded on a daily basis and expressed as the mean percent changes of infected animals (A). For the second experiment, 10 Tg^+ AC63 mice were inoculated (i.n.) with 10^6 $TCID_{50}$ of SARS-CoV. Five mice and three infected mice were sacrificed at days 5 and 8 after infection, respectively, and the titers of infectious virus in the lungs and brains were assessed and expressed as log_{10}/gram (B). The other two infected mice were saved for observation of weight changes (C) and other clinical manifestations. **, $P < 0.01$ by Student's t test, comparing the virus titers between lungs and brain within Tg^+ or Tg^- mice.

and generalized illness, along with tissue pathology and inflammatory cytokine responses. Most significantly, transgenic AC70 mice developed clinical illness, regardless of the route of inoculation, and died uniformly within 8 days after infection, whereas transgenic AC63 mice eventually recovered from the infection, despite the manifestations of clinical illness.

Mice transgenic for hACE2 exhibit distinct clinical courses following SARS-CoV infection which are not seen in infected wild-type mice. SARS-CoV infection in the BALB/c and C57BL/6 strains appeared to be short lived, with the viral clearance occurring within 4 to 8 days after infection. It is noteworthy that these infected wild-type strains of mouse did not elicit a specific antibody response to SARS-CoV until days 21 to 28 after infection. Furthermore, mutant mice lacking key immune components, including $RAG1^{-/-}$, $CD1^{-/-}$, and $bg^{-/-}$ mice, were shown to clear the infections as efficiently as wild-type mice, suggesting that the classic host antiviral immune responses might not be critical for resolving SARS-CoV infection in the mouse. Although a prolonged replication of SARS-CoV accompanied by the onset of clinical illness was observed in $Stat1^{-/-}$ mice, the patterns of the clinical manifestations appeared to be atypical, in which no evidence of acute inflammatory response in any organ could be observed. Nevertheless, the compromised ability of Stat1-deficient mice to clear virus highlights the importance of innate immunity in controlling SARS-CoV infection in the mouse (9, 12, 36). Furthermore, as BALB/c mice 1 year of age or older were more susceptible than younger mice to SARS-CoV, resulting in the development of a limited and nonfatal illness showing increased pathological changes in the respiratory tract, age is a key determinant of the susceptibility to SARS in animals as in the case for humans (3, 28, 42). Here again, contrary to the severe and often fatal outcome of SARS in elderly patients, aged mice effectively recovered from the disease, without any mortality. Thus, our transgenic mouse model is unique in that it provides defined end-points, including death, weight loss, and respiratory and neurological symptoms as well as virological data and pathological changes, and thus allows for the definitive analysis of the efficacy of antivirals and vaccines to SARS.

Studies of the kinetics and tissue distribution of viral replication in i.n.-challenged AC70 mice demonstrated that the lungs are the major sites of SARS-CoV replication before dissemination to other tissues, particularly the brain (Fig. 3 and

4). Despite the resemblance in the kinetics of viral replication in the lungs, Tg^+ mice appear to be more efficient than their Tg^- littermates at supporting viral replication, resulting in a more intense pulmonary infection. Virus subsequently spread from the lungs to the brain of Tg^+ mice at day 2; actively replicated there, reaching its maximal level at day 3; and was sustained thereafter until the death of the hosts. The extensive pulmonary and CNS involvement in infected AC70 Tg^+ mice was confirmed by IHC, which readily revealed the expression of SARS-CoV antigen in patches of pneumocytes and bronchial epithelial cells, as well as in neuronal and glial cells (Fig. 5). Importantly, the expression of viral antigen in the lungs, brain, and GI tracts generally correlated with hACE2 expression (Fig. 5 and 6). However, whether hACE2 and viral antigen could be detected in the same cells remains unknown. Interestingly, not all hACE2-expressing cells in Tg^+ AC70 mice were susceptible to SARS-CoV infection. For instance, we were unable to detect SARS-CoV infection in cells lining the endothelium of various organs, despite their intense hACE2 expression (Fig. 6), an observation consistent with the finding with clinical specimens (11, 39). The reason for the lack of SARS-CoV infection in cells highly positive for hACE2 expression in our transgenic animals is not known, but this observation supports the notion that the expression of hACE2 alone might not be sufficient for maintaining effective viral infection (39). The finding of L-SIGN as another cellular receptor for SARS-CoV (16) might imply that other receptors or coreceptors might be required for viral entry into different cells. It is also possible that surface expression of hACE2 is not present, as shown for Calu-3 cells (41), making those cells insusceptible for SARS-CoV infection. Other host factors, such as pH values, temperature, and oxygen levels, have been implicated in pH-dependent cell entry of poliovirus and rhinovirus (45) and may be also important in defining the tissue tropism of SARS-CoV, which has been shown to be related to pH-dependent cell entry in vitro (27, 49).

SARS is generally recognized as an acute viral pneumonia with the lungs as its main pathological target. However, like other human and animal coronaviruses, many of which are known to establish acute and persistent infections in neural cells (1, 2, 4, 15), SARS-CoV has been detected by RT-PCR, in situ hybridization, and IHC in the brains and other extrapulmonary tissues of patients who died of SARS (5, 10, 11, 47). This neurotropic potential of SARS-CoV is underscored by the recent findings in an experimental mouse model, in which infectious virus was recovered from the brains of infected C57BL/6 mice (9). Also, several neuronal cell lines of human or rat origins, as well as human glioma cell lines, are permissive for SARS-CoV replication (48; C.-T. Tseng and N. Wang, unpublished data). Thus, the identification of the brain as a major extrapulmonary site of SARS-CoV infection, particularly in Tg^+ mice, falls within the spectrum of coronavirus pathogenesis.

It has been well established that the spread of respiratory viruses to the brain could be mediated either directly through synaptically linked neurons of the olfactory and trigeminal systems, as described in the animal models for Venezuelan equine encephalitis virus, pseudorabies virus, and avian influenza virus A (H5N1) infection (8, 14, 25, 33), or through the hematogenous route, via the damaged blood-brain barrier. Although the exact route or routes of SARS-CoV dissemination to the CNS remain to be determined, the revelation of low-level viremia in infected (i.n.) Tg^+ mice at day 2, along with the detection of high virus titers in the brains, but not in the lungs, of i.p.-challenged Tg^+ mice might provide the basis for a hematogenous route of viral transmission.

Autopsy studies have indicated that DAD is the most characteristic pathology in SARS (6, 7, 11, 26). While SARS-associated DAD could be caused directly by viral destruction of permissive cells lining the alveoli, the marked heterogeneity of the disease course and the outcome of the infection suggest that host responses may play an important role in the pathogenesis of SARS. Specifically, elevated and prolonged expression of inflammatory mediators, such as CCL2/MIP-1, CXCL8, CXCL9, and CXCL10/IP-10, have been found in SARS patients and experimentally infected (i.n.) C57BL/6 mice (9, 10, 13, 42, 44, 46). Although an early enhanced expression of IP-10 has been implicated to be an prognostic indicator for the adverse outcome of SARS-CoV infection (38), the exact protective and/or pathological nature and the spectrum of such exaggerated inflammatory responses in the lungs of SARS patients, especially during the early stages of the infection, have never been explored, as invasive procedures required for such studies were not possible during such an explosive outbreak. Therefore, the robust and highly sustainable SARS-CoV infection in our transgenic mouse model makes it unique for investigation of the inflammatory responses within the local tissues: i.e., the lungs and brain.

In contrast to Tg^- mice that failed to elicit significant inflammatory responses to SARS-CoV infection, infected Tg^+ mice promptly released elevated levels of IL-1β, IL-12_{p40}, CXCL1/KC, CCL5/RANTES, CCL2/MIP-1, and IL-12_{p70} within the lungs at days 1 and 2 p.i. (Fig. 7). Although such an acute host inflammatory response did not occur in the brain at day 2, intense secretion of the aforementioned inflammatory mediators, as well as IL-6, granulocyte-colony stimulation factor (G-CSF), CCL3/MIP-1α, IL-1α, and granulocyte/monocyte colony stimulating factor (GM-CSF), was detected at day 3 (Table 1), concurrently with a marked elevation in the amount of infectious virus.

Despite the extensive involvement in the viral infection and the subsequent inflammatory secretion of the CNS, neither necrosis nor cellular infiltrates could be observed in this vital tissue at this stage of the infection. It has been shown that primary cultures of mouse neurons, astrocytes, and microglia were capable of producing innate inflammatory cytokines in response to neurovirulent mouse hepatitis virus JHM infection (30). Thus, the absence of leukocyte infiltrates in the brains of infected Tg^+ mice at day 3 might suggest that the resident brain cells are the likely source of these innate inflammatory cytokines. Although the significance of these inflammatory cytokines and chemokines in the pathogenesis of SARS-CoV infection in this transgenic mouse model is currently unknown, some morphologically subtle changes in the CNS of infected Tg^+ mice may underlie inflammatory cytokine- and chemokine-mediated functional derangement of the CNS (29, 43), which could be central to the pathogenesis of SARS-CoV infection. Preliminary studies of SARS-CoV infection with mice of the AC63 line indicated that this lineage was also permissive to infection but resistant to the fatal outcome of

SARS-CoV infection (Fig. 8). Whether lower hACE2 expression in the AC63 line compared to that in AC70 (Fig. 1) could be responsible for their recovery and survival remains to be studied.

In summary, we have demonstrated in this study that transgenic mice expressing hACE2 are highly susceptible to SARS-CoV infection, resulting in a wide spectrum of clinical manifestations, including death, depending upon the transgenic lineages. We believe that these transgenic mice will be useful for studying the pathogenesis of SARS and preclinical testing of antiviral agents and vaccine candidates against SARS.

ACKNOWLEDGMENTS

This work was supported by grants and contracts from the NIH (NO1 AI25489 to C.J.P., AI29984 to S.M., and AI063118 to T.C.) and the endowment fund of John Sealy Distinguished University Chair in Tropical & Emerging Virology (to C.J.P.). C.H. was supported by the James W. McLaughlin Fellowship Fund.

We thank Yoshihiro Kawaoka for kindly providing the expression vector and Missy Worthy and Yueqing Zhang for excellent technical support.

REFERENCES

1. **Arbour, N., G. Côté, C. Lachance, M. Tardieu, N. R. Cashman, and P. J. Talbot.** 1999. Acute and persistent infection of human neural cell lines by human coronavirus OC43. J. Virol. **73:**3338–3350.
2. **Butler, N., L. Pewe, K. Trandem, and S. Perlman.** 2006. Murine encephalitis caused by HCoV-OC43, a human coronavirus with broad species specificity, is partly immune-mediated. Virology **347:**410–421.
3. **Chan, K. S., J. P. Zheng, Y. W. Mok, Y. M. Li, Y. N. Liu, C. M. Chu, and M. S. Ip.** 2003. SARS: prognosis, outcome and sequelae. Respirology **8:**(Suppl.) S36–S40.
4. **Coley, S. E., E. Lavi, S. G. Sawicki, L. Fu, B. Schelle, N. Karl, S. G. Siddell, and V. Thiel.** 2005. Recombinant mouse hepatitis virus strain A59 from cloned, full-length cDNA replicates to high titers in vitro and is fully pathogenic in vivo. J. Virol. **79:**3097–3106.
5. **Ding, Y., L. He, Q. Zhang, Z. Huang, X. Che, J. Hou, H. Wang, H. Shen, L. Qiu, Z. Li, J. Geng, J. Cai, H. Han, X. Li, W. Kang, D. Weng, P. Liang, and S. Jiang.** 2004. Organ distribution of severe acute respiratory syndrome (SARS) associated coronavirus (SARS-CoV) in SARS patients: implications for pathogenesis and virus transmission pathways. J. Pathol. **203:**622–630.
6. **Ding, Y., H. Wang, H. Shen, Z. Li, J. Geng, H. Han, J. Cai, X. Li, W. Kang, D. Weng, Y. Lu, D. Wu, L. He, and K. Yao.** 2003. The clinical pathology of severe acute respiratory syndrome (SARS): a report from China. J. Pathol. **200:**282–289.
7. **Franks, T. J., P. Y. Chong, P. Chui, J. R. Galvin, R. M. Lourens, A. H. Reid, E. Selbs, C. P. McEvoy, C. D. Hayden, J. Fukuoka, J. K. Taubenberger, and W. D. Travis.** 2003. Lung pathology of severe acute respiratory syndrome (SARS): a study of 8 autopsy cases from Singapore. Hum. Pathol. **34:**743–748.
8. **Gerdts, V., J. Beyer, B. Lomniczi, and T. C. Mettenleiter.** 2000. Pseudorabies virus expressing bovine herpesvirus 1 glycoprotein B exhibits altered neurotropism and increased neurovirulence. J. Virol. **74:**817–827.
9. **Glass, W. G., K. Subbarao, B. Murphy, and P. M. Murphy.** 2004. Mechanisms of host defense following severe acute respiratory syndrome-coronavirus (SARS-CoV) pulmonary infection of mice. J. Immunol. **173:**4030–4039.
10. **Gu, J., E. Gong, B. Zhang, J. Zheng, Z. Gao, Y. Zhong, W. Zou, J. Zhan, S. Wang, Z. Xie, H. Zhuang, B. Wu, H. Zhong, H. Shao, W. Fang, D. Gao, F. Pei, X. Li, Z. He, D. Xu, X. Shi, V. M. Anderson, and A. S. Leong.** 2005. Multiple organ infection and the pathogenesis of SARS. J. Exp. Med. **202:**415–424.
11. **Hamming, I., W. Timens, M. L. Bulthuis, A. T. Lely, G. J. Navis, and H. van Goor.** 2004. Tissue distribution of ACE2 protein, the functional receptor for SARS coronavirus. A first step in understanding SARS pathogenesis. J. Pathol. **203:**631–637.
12. **Hogan, R. J., G. Gao, T. Rowe, P. Bell, D. Flieder, J. Paragas, G. P. Kobinger, N. A. Wivel, R. G. Crystal, J. Boyer, H. Feldmann, T. G. Voss, and J. M. Wilson.** 2004. Resolution of primary severe acute respiratory syndrome-associated coronavirus infection requires Stat1. J. Virol. **78:**11416–11421.
13. **Huang, K. J., I. J. Su, M. Theron, Y. C. Wu, S. K. Lai, C. C. Liu, and H. Y. Lei.** 2005. An interferon-gamma-related cytokine storm in SARS patients. J. Med. Virol. **75:**185–194.
14. **Iwasaki, T., S. Itamura, H. Nishimura, Y. Sato, M. Tashiro, T. Hashikawa, and T. Kurata.** 2004. Productive infection in the murine central nervous system with avian influenza virus A (H5N1) after intranasal inoculation. Acta Neuropathol. (Berlin) **108:**485–492.
15. **Jacomy, H., G. Fragoso, G. Almazan, W. E. Mushynski, and P. J. Talbot.** 2006. Human coronavirus OC43 infection induces chronic encephalitis leading to disabilities in BALB/c mice. Virology **349:**335–346.
16. **Jeffers, S. A., S. M. Tusell, L. Gillim-Ross, E. M. Hemmila, J. E. Achenbach, G. J. Babcock, W. D. Thomas, Jr., L. B. Thackray, M. D. Young, R. J. Mason, D. M. Ambrosino, D. E. Wentworth, J. C. Demartini, and K. V. Holmes.** 2004. CD209L (L-SIGN) is a receptor for severe acute respiratory syndrome coronavirus. Proc. Natl. Acad. Sci. USA **101:**15748–15753.
17. **Ksiazek, T. G., D. Erdman, C. S. Goldsmith, S. R. Zaki, T. Peret, S. Emery, S. Tong, C. Urbani, J. A. Comer, W. Lim, P. E. Rollin, S. F. Dowell, A. E. Ling, C. D. Humphrey, W. J. Shieh, J. Guarner, C. D. Paddock, P. Rota, B. Fields, J. DeRisi, J. Y. Yang, N. Cox, J. M. Hughes, J. W. LeDuc, W. J. Bellini, and L. J. Anderson.** 2003. A novel coronavirus associated with severe acute respiratory syndrome. N. Engl. J. Med. **348:**1953–1966.
18. **Kuiken, T., R. A. Fouchier, M. Schutten, G. F. Rimmelzwaan, G. van Amerongen, D. van Riel, J. D. Laman, T. de Jong, G. van Doornum, W. Lim, A. E. Ling, P. K. Chan, J. S. Tam, M. C. Zambon, R. Gopal, C. Drosten, S. van der Werf, N. Escriou, J. C. Manuguerra, K. Stohr, J. S. Peiris, and A. D. Osterhaus.** 2003. Newly discovered coronavirus as the primary cause of severe acute respiratory syndrome. Lancet **362:**263–270.
19. **Lau, S. K., P. C. Woo, K. S. Li, Y. Huang, H. W. Tsoi, B. H. Wong, S. S. Wong, S. Y. Leung, K. H. Chan, and K. Y. Yuen.** 2005. Severe acute respiratory syndrome coronavirus-like virus in Chinese horseshoe bats. Proc. Natl. Acad. Sci. USA **102:**14040–14045.
20. **Li, W., M. J. Moore, N. Vasilieva, J. Sui, S. K. Wong, M. A. Berne, M. Somasundaran, J. L. Sullivan, K. Luzuriaga, T. C. Greenough, H. Choe, and M. Farzan.** 2003. Angiotensin-converting enzyme 2 is a functional receptor for the SARS coronavirus. Nature **426:**450–454.
21. **Li, W., Z. Shi, M. Yu, W. Ren, C. Smith, J. H. Epstein, H. Wang, G. Crameri, Z. Hu, H. Zhang, J. Zhang, J. McEachern, H. Field, P. Daszak, B. T. Eaton, S. Zhang, and L. F. Wang.** 2005. Bats are natural reservoirs of SARS-like coronaviruses. Science **310:**676–679.
22. **Li, W., S.-K. Wong, F. Li, J. H. Kuhn, I.-C. Huang, H. Choe, and M. Farzan.** 2006. Animal origins of the severe acute respiratory syndrome coronavirus: insight from ACE2–S-protein interactions. J. Virol. **80:**4211–4219.
23. **Martina, B. E., B. L. Haagmans, T. Kuiken, R. A. Fouchier, G. F. Rimmelzwaan, G. van Amerongen, J. S. Peiris, W. Lim, and A. D. Osterhaus.** 2003. Virology: SARS virus infection of cats and ferrets. Nature **425:**915.
24. **Mossel, E. C., C. Huang, K. Narayanan, S. Makino, R. B. Tesh, and C. J. Peters.** 2005. Exogenous ACE2 expression allows refractory cell lines to support severe acute respiratory syndrome coronavirus replication. J. Virol. **79:**3846–3850.
25. **Mulder, W., J. Pol, T. Kimman, G. Kok, J. Priem, and B. Peeters.** 1996. Glycoprotein D-negative pseudorabies virus can spread transneuronally via direct neuron-to-neuron transmission in its natural host, the pig, but not after additional inactivation of gE or gI. J. Virol. **70:**2191–2200.
26. **Nicholls, J. M., L. L. Poon, K. C. Lee, W. F. Ng, S. T. Lai, C. Y. Leung, C. M. Chu, P. K. Hui, K. L. Mak, W. Lim, K. W. Yan, K. H. Chan, N. C. Tsang, Y. Guan, K. Y. Yuen, and J. S. Peiris.** 2003. Lung pathology of fatal severe acute respiratory syndrome. Lancet **361:**1773–1778.
27. **Nie, Y., P. Wang, X. Shi, G. Wang, J. Chen, A. Zheng, W. Wang, Z. Wang, X. Qu, M. Luo, L. Tan, X. Song, X. Yin, J. Chen, M. Ding, and H. Deng.** 2004. Highly infectious SARS-CoV pseudotyped virus reveals the cell tropism and its correlation with receptor expression. Biochem. Biophys. Res. Commun. **321:**994–1000.
28. **Peiris, J. S., K. Y. Yuen, A. D. Osterhaus, and K. Stohr.** 2003. The severe acute respiratory syndrome. N. Engl. J. Med. **349:**2431–2441.
29. **Peterson, K. E., and B. Chesebro.** 2006. Influence of proinflammatory cytokines and chemokines on the neuropathogenesis of oncornavirus and immunosuppressive lentivirus infections. Curr. Top. Microbiol. Immunol. **303:**67–95.
30. **Rempel, J. D., L. A. Quina, P. K. Blakely-Gonzales, M. J. Buchmeier, and D. L. Gruol.** 2005. Viral induction of central nervous system innate immune responses. J. Virol. **79:**4369–4381.
31. **Roberts, A., C. Paddock, L. Vogel, E. Butler, S. Zaki, and K. Subbarao.** 2005. Aged BALB/c mice as a model for increased severity of severe acute respiratory syndrome in elderly humans. J. Virol. **79:**5833–5838.
32. **Roberts, A., L. Vogel, J. Guarner, N. Hayes, B. Murphy, S. Zaki, and K. Subbarao.** 2005. Severe acute respiratory syndrome coronavirus infection of golden Syrian hamsters. J. Virol. **79:**503–511.
33. **Ryzhikov, A. B., E. I. Ryabchikova, A. N. Sergeev, and N. V. Tkacheva.** 1995. Spread of Venezuelan equine encephalitis virus in mice olfactory tract. Arch. Virol. **140:**2243–2254.
34. **Shieh, W. J., C. H. Hsiao, C. D. Paddock, J. Guarner, C. S. Goldsmith, K. Tatti, M. Packard, L. Mueller, M. Z. Wu, P. Rollin, I. J. Su, and S. R. Zaki.** 2005. Immunohistochemical, in situ hybridization, and ultrastructural localization of SARS-associated coronavirus in lung of a fatal case of severe acute respiratory syndrome in Taiwan. Hum. Pathol. **36:**303–309.
35. **Song, H. D., C. C. Tu, G. W. Zhang, S. Y. Wang, K. Zheng, L. C. Lei, Q. X. Chen, Y. W. Gao, H. Q. Zhou, H. Xiang, H. J. Zheng, S. W. Chern, F. Cheng,**

C. M. Pan, H. Xuan, S. J. Chen, H. M. Luo, D. H. Zhou, Y. F. Liu, J. F. He, P. Z. Qin, L. H. Li, Y. Q. Ren, W. J. Liang, Y. D. Yu, L. Anderson, M. Wang, R. H. Xu, X. W. Wu, H. Y. Zheng, J. D. Chen, G. Liang, Y. Gao, M. Liao, L. Fang, L. Y. Jiang, H. Li, F. Chen, B. Di, L. J. He, J. Y. Lin, S. Tong, X. Kong, L. Du, P. Hao, H. Tang, A. Bernini, X. J. Yu, O. Spiga, Z. M. Guo, H. Y. Pan, W. Z. He, J. C. Manuguerra, A. Fontanet, A. Danchin, N. Niccolai, Y. X. Li, C. I. Wu, and G. P. Zhao. 2005. Cross-host evolution of severe acute respiratory syndrome coronavirus in palm civet and human. Proc. Natl. Acad. Sci. USA **102:**2430–2435.

36. **Subbarao, K., J. McAuliffe, L. Vogel, G. Fahle, S. Fischer, K. Tatti, M. Packard, W.-J. Shieh, S. Zaki, and B. Murphy.** 2004. Prior infection and passive transfer of neutralizing antibody prevent replication of severe acute respiratory syndrome coronavirus in the respiratory tract of mice. J. Virol. **78:**3572–3577.
37. **Subbarao, K., and A. Roberts.** 2006. Is there an ideal animal model for SARS? Trends Microbiol. **14:**299–303.
38. **Tang, N. L., P. K. Chan, C. K. Wong, K. F. To, A. K. Wu, Y. M. Sung, D. S. Hui, J. J. Sung, and C. W. Lam.** 2005. Early enhanced expression of interferon-inducible protein-10 (CXCL-10) and other chemokines predicts adverse outcome in severe acute respiratory syndrome. Clin. Chem. **51:**2333–2340.
39. **To, K. F., J. H. Tong, P. K. Chan, F. W. Au, S. S. Chim, K. C. Chan, J. L. Cheung, E. Y. Liu, G. M. Tse, A. W. Lo, Y. M. Lo, and H. K. Ng.** 2004. Tissue and cellular tropism of the coronavirus associated with severe acute respiratory syndrome: an in-situ hybridization study of fatal cases. J. Pathol. **202:**157–163.
40. **Tseng, C. T., L. A. Perrone, H. Zhu, S. Makino, and C. J. Peters.** 2005. Severe acute respiratory syndrome and the innate immune responses: modulation of effector cell function without productive infection. J. Immunol. **174:**7977–7985.
41. **Tseng, C.-T. K., J. Tseng, L. Perrone, M. Worthy, V. Popov, and C. J. Peters.** 2005. Apical entry and release of severe acute respiratory syndrome-associated coronavirus in polarized Calu-3 lung epithelial cells. J. Virol. **79:**9470–9479.
42. **Tsui, S. K., S. S. Chim, and Y. M. Lo.** 2003. Coronavirus genomic-sequence variations and the epidemiology of the severe acute respiratory syndrome. N. Engl. J. Med. **349:**187–188.
43. **Wang, T., J. A. Rumbaugh, and A. Nath.** 2006. Viruses and the brain: from inflammation to dementia. Clin. Sci. (London) **110:**393–407.
44. **Ward, S. E., M. R. Loutfy, L. M. Blatt, K. A. Siminovitch, J. Chen, A. Hinek, B. Wolff, D. H. Pham, H. Deif, E. A. LaMere, K. C. Kain, G. A. Farcas, P. Ferguson, M. Latchford, G. Levy, L. Fung, J. W. Dennis, E. K. Lai, and E. N. Fish.** 2005. Dynamic changes in clinical features and cytokine/chemokine responses in SARS patients treated with interferon alfacon-1 plus corticosteroids. Antivir. Ther. **10:**263–275.
45. **Whitton, J. L., C. T. Cornell, and R. Feuer.** 2005. Host and virus determinants of picornavirus pathogenesis and tropism. Nat. Rev. Microbiol. **3:**765–776.
46. **Wong, C. K., C. W. Lam, A. K. Wu, W. K. Ip, N. L. Lee, I. H. Chan, L. C. Lit, D. S. Hui, M. H. Chan, S. S. Chung, and J. J. Sung.** 2004. Plasma inflammatory cytokines and chemokines in severe acute respiratory syndrome. Clin. Exp. Immunol. **136:**95–103.
47. **Xu, J., S. Zhong, J. Liu, L. Li, Y. Li, X. Wu, Z. Li, P. Deng, J. Zhang, N. Zhong, Y. Ding, and Y. Jiang.** 2005. Detection of severe acute respiratory syndrome coronavirus in the brain: potential role of the chemokine Mig in pathogenesis. Clin. Infect. Dis. **41:**1089–1096.
48. **Yamashita, M., M. Yamate, G. M. Li, and K. Ikuta.** 2005. Susceptibility of human and rat neural cell lines to infection by SARS-coronavirus. Biochem. Biophys. Res. Commun. **334:**79–85.
49. **Yang, Z.-Y., Y. Huang, L. Ganesh, K. Leung, W.-P. Kong, O. Schwartz, K. Subbarao, and G. J. Nabel.** 2004. pH-dependent entry of severe acute respiratory syndrome coronavirus is mediated by the spike glycoprotein and enhanced by dendritic cell transfer through DC-SIGN. J. Virol. **78:**5642–5650.